

## Preparation and Characterization of Nanoporous Zeolitic Membranes for Catalytic Applications

Dr. Talib M. Naieff Al-Bayati

Chemical Engineering Department, University of Technology/Baghdad

Email: talib\_albyati@yahoo.com

Received on: 25/3/2013 & Accepted on: 15/8/2013

### ABSTRACT

The Hydroisomerization and Hydrocracking of n-Heptane was carried out in a packed bed plug-flow zeolitic catalytic membrane reactor at a constant pressure of (100 kpa). Material was encapsulated by trimetallic 1% (Pt-Ni-Co). The structural and textural features for encapsulated nanoporous MCM-48 were studied by X-ray diffraction, scanning electron microscopy (SEM), EDAX, nitrogen adsorption-desorption (BET) and FTIR. The characterizations were carried out before and after loading.

The results show that the catalytic activity evaluation in a membrane reactor revealed that trimetallic 1% (Pt-Ni-Co)/MCM-48 catalyst possess a high activity for conversion of n-heptane around (83%) at 400 °C with a maximum selectivity around (65%) at 325 °C.

**Keywords:** Nanoporous material; MCM-48; Membrane reactor; n-heptane; trimetallic catalyst; hydroisomerization; hydrocracking.

### تحضير وفحص خصائص الغشاء الزيولائي النانوي المسامي لتطبيقات التحفيز

#### الخلاصة

ان عملية الازمرة والتكسير الحراري قد اجريت في المفاعل الغشائي الزيولائي ذو الطبقة المحشوة عند ضغط ثابت بحدود (100 كيلو باسكال) باستخدام MCM-48 التي تم تحميلها بالمعادن الثلاثية 1% (البلاتين-النيكل-الكوبلت). ان تركيب المادة ومميزات السطح الخارجي تم دراستها بواسطة الاشعة السينية XRD بالاضافة الى دراسة المسح الالكتروني المجهر SEM وتحليل نسبة العناصر EDAX. وكما تم قياس المساحة السطحية وقطر المسامات بواسطة غاز النيتروجين بعملية الامدصاص وازالة الامدصاص BET. بالاضافة الى قياس المجاميع الفعالة FT-IR ان جميع هذه الخصائص تم دراستها قبل وبعد عملية التحميل بالمعادن. اظهرت النتائج ان فعالية تقييم العامل المساعد في المفاعل الغشائي توحى بان المعادن الثلاثية المحملة (Pt-Ni-Co)/MCM-48 0.1% لها فعالية عالية اثناء تحويل الهبتان الاعتيادي بحدود 83% في المفاعل الغشائي في درجة حرارة 400 م° مع اقصى انتقائية بحدود 65% في درجة حرارة 325 م°.

## INTRODUCTION

Isomerization of paraffins is a refinery process that generates high octane for the gasoline pool, while contributing no olefins or aromatics. Branched C<sub>5</sub> and C<sub>6</sub> paraffins have much higher octanes than normal pentane and normal hexane as indicated in Table (1). Furthermore, lower octane C<sub>5</sub> and C<sub>6</sub> isomers can be separated, and recycled.

**Table (1) Octane and boiling points for C<sub>5</sub> and C<sub>6</sub> paraffin's [1].**

Paraffin	*(RON+MON)/2	Boiling Point, °C
Isopentane	102.0	27.9
Normal Pentane	64.0	36.1
2,2-Dimethylbutane	93.0	49.7
2,3-Dimethylbutane	101.0	58.0
2-Methylpentane	80.0	60.3
3-Methylpentane	83.0	63.3
Normal Hexane	20.5	68.7

\* **RON** is Research Octane Number & **MON** is Motor Octane Number

Skeletal isomerization of n-paraffins is an acid-catalyzed reaction that is thermodynamically favored at lower temperature. The goal therefore has to be maximizing gasoline octane with recycle flow schemes and with catalysts that are active at low temperatures. Catalysts also must have high selectivity to isomerization in order to maximize gasoline yield. Zeolitic membrane molecular sieves can be utilized to recycle normal paraffins at high energy efficiency compared to fractionation [1, 2].

There are numerous examples for the application of zeolite membranes to enhance a chemical reaction like de-hydrogenation, partial oxidation, isomerization or esterification. The traditional applications of zeolite membranes in reactors are focused on conversion enhancement by equilibrium displacement or by selectively removing reaction rate inhibitors [3]. In the last decade, supported zeolite layers have attracted intensive research efforts due to their potential applications as separation membrane, catalytic membrane reactor, chemical sensor, electrode, opto-electronic device, low dielectric constant material for use as electrical insulator, protection or insulation layer or as host for the organization of functional guest molecules. Recently several pioneering papers on the prospects of zeolite films beyond the realm of separation for assembly of novel and complex functional materials including molecular sensors, mechanically stable dielectrics, and novel reaction-diffusion devices appeared [4–10]. Ordered porous molecular sieve layers are believed to be important materials in the nanotechnology era with novel emerging applications [11, 12].

The discovery of mesoporous material MCM-48, in 1992 by the Mobil Oil researchers has attracted much research attention owing to their potential applications as catalysts, catalyst supports and absorbents. Characteristic properties of this material are large surface areas (1000-1500 m<sup>2</sup>g<sup>-1</sup>), specific

pore volume up to  $1.2 \text{ cm}^3\text{g}^{-1}$ , high thermal stability, a narrow pore-size distribution and “non-cytotoxic” properties [13-21] as shown in Figure (1).

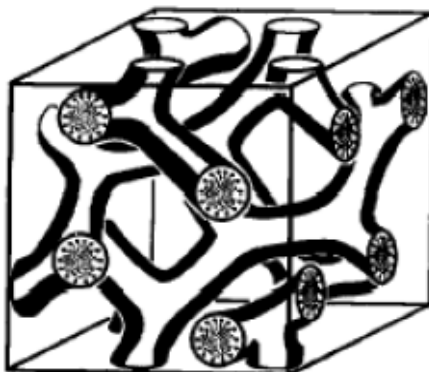


Figure (1) Schematic diagram for cubic nanoporous material MCM-48[22].

Because of the aforementioned characterization of MCM-48 the aim of this research was devoted to use it in hydroisomerization and hydrocracking reaction process in membrane reactor. However, no more studies have so far been reported in the open literature on the use of Nanoporous trimetallic catalysts for isomerization and reforming processes of n-Heptane. In this work, the catalytic activities have been investigated of 1 % (Pt-Ni-Co) catalysts supported on MCM-48 as a membrane reactor for the reaction of n-heptane in Hydroisomerization and Hydrocracking reactions.

## EXPERIMENTAL

### Chemicals

Triblock copolymer poly (ethylene glycol)- Block-poly (propylene glycol)-block-poly (ethylene glycol) (Pluronic P123, molecular weight = 5800, EO<sub>20</sub>PO<sub>70</sub>EO<sub>20</sub>), tetraethyl orthosilicate (TEOS; purity > 98 %) as a silica source), cetyltrimethylammonium bromide (CTAB; purity > 98%) as a surfactant, hydrochloric acid (HCl), Pt (NH<sub>3</sub>)<sub>4</sub>Cl<sub>2</sub>.H<sub>2</sub>O (99.99 %), CoN<sub>2</sub>O<sub>6</sub>.6H<sub>2</sub>O (99.99 %), and Ni (NO<sub>3</sub>)<sub>2</sub>.6H<sub>2</sub>O (99.99 %), ( 99%) were supplied by Aldrich Chemical Inc., n-Heptane's (purity of 99.33 wt. %:Sigma-Aldrich). All chemicals were used as received without further purification. Millipore water was used in all experiments.

### Synthesis of MCM-48

MCM-48 was prepared according to the synthesis procedure described by [23-24]. In a representative synthesis, MCM-48 was prepared as follows: 10 g of CTAB was mixed with 90 g of deionized water and the mixture was vigorously stirred at 35 °C for 40 min, then 1g of NaOH was added to the mixture. 60 min of vigorous stirring at 35 °C after, 11 cm<sup>3</sup> of TEOS was added to the mixture and the stirring continued at 35 C for 30 min. Finally, the mixture was heated for 24h at 150 °C in an autoclave under a static condition; the resulting MCM-48 product was cooled for 1 hr then filtered, washed with distilled water and dried at room

temperatures. The purified synthesized sample was then calcined for 6 h at 650 °C using a heating ramp rate of 2 °C/min.

#### Preparation of Metals Support MCM-48 Mesoporous Catalyst

MCM-48 samples were metal-loaded by incipient wetness impregnation (IWI) with  $\text{Pt}(\text{NH}_3)_4\text{Cl}_2 \cdot \text{H}_2\text{O}$  as a platinum precursor,  $\text{Ni}(\text{NO}_3)_2 \cdot 6\text{H}_2\text{O}$  as a nickel precursor and  $\text{Co}(\text{NO}_3)_2 \cdot 6\text{H}_2\text{O}$  as a cobalt precursor. Impregnation solutions were prepared by dissolving appropriate amount of metal salt (1% loading) is introduced into 0.1 M HCl solvent to load metals with a total of 1 wt% Pt, Ni and Co. In order to achieve a high metal dispersion and inhibit agglomeration of particles during vaporization of metal salt solution, the total volume of solution was used equal to that of the total pore volume of the support. After impregnation, the catalysts were dried overnight at ambient temperature, and then the sample is dried in oven for 24 h at 120 °C, and after that the catalyst was calcined at 500 °C for 4 h [24].

#### Synthesis of 1 % (Pt-Ni-Co)/MCM-48 Membranes

Before loading into the micro-reactor, it is necessary to press the catalyst to a disk shape. The molding was achieved by packing 0.2 g (Pt-Ni-Co)/MCM-48 into the mold and then inserted into the pneumatic press pumped approximately (10 tones/cm<sup>2</sup>) for 10 minutes, and then the disk shape was formed.

The pressed catalyst is loaded into a cylindrical Pyrex micro-reactor of 4 mm ID and 400 mm length. Sufficient glass wool is inserted into the reactor as a support. This is placed into the reactor with a center distance at 15 cm from the top of the micro-reactor, and then more glass wool is inserted from the top into the micro-reactor to hold the catalyst in place as shown in Figure (2).

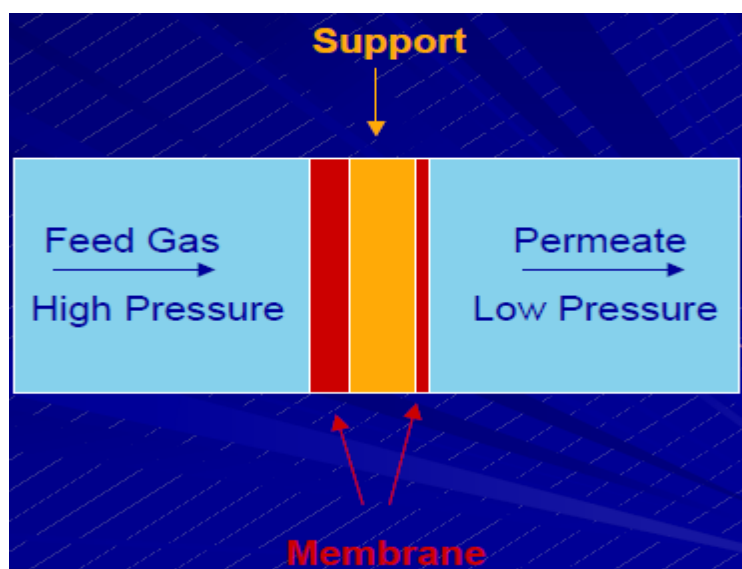


Figure (2) Schematic diagram for a disk 1% (Pt-Ni-Co)/MCM-48 membrane.

#### Characterization

The small-angle XRD patterns were recorded under ambient conditions on a MiniFlex (Rigaku) diffractometer with Cu K $\alpha$  radiation ( $\lambda = 1.5406\text{\AA}$ ). The X-ray tube was operated at 40 kV and 30 mA while the data were recorded in the  $2\theta$  range of  $0.5\text{--}8^\circ$  with a  $2\theta$  step size of 0.01 and a step time of 10s. Nitrogen adsorption/desorption measurements were conducted using a Micrometrics ASAP 2020 pore analyzer by N<sub>2</sub> physisorption at  $-196^\circ\text{C}$ . All samples were degassed for 3 h at  $350^\circ\text{C}$  under vacuum ( $p < 10^{-5}$  mbar) in the degas port of the sorption analyzer. The BET specific surface area of the samples was calculated using the Brunauer–Emmett–Teller (BET) method in the range of relative pressures between 0.05 and 0.25. The pore size distributions were calculated from the desorption branch of the isotherm using the thermodynamics-based Barrett–Joyner–Halenda (BJH) method. The total pore volume was determined from the adsorption branch of the N<sub>2</sub> isotherm as the amount of liquid nitrogen adsorbed at  $P/P_0 = 0.995$ . Mean mesopore diameters for the various samples were estimated from the nitrogen sorption data using BET analysis (4V/A). The macropore structure was characterized by scanning electron microscopy (SEM), performed on a JEOL (JSM-5600 LV) scanning electron microscope. EDAX used in combination with SEM is an analytical technique which forms an elemental analysis of the catalyst to identify the chemical composition. The infrared spectra (FT-IR) of the solid samples, diluted in (8 wt. %) KBr were recorded at room temperature in transmission mode in the range of  $4000$  to  $400\text{ cm}^{-1}$  at  $4\text{ cm}^{-1}$  resolution regions using NICOLET 380 FT-IR spectrometer.

#### Catalytic Test and Gas Permeation Measurements

0.1 g of (Pt-Ni-Co/MCM-48) a disk catalyst was loaded into a cylindrical fixed bed Pyrex micro-membrane reactor of 4 mm ID and 400 mm length and held in place in the reactor by glass wool as a support. The catalysts were calcined in air and reduced in H<sub>2</sub> in situ with  $50\text{ ml min}^{-1}$  air/H<sub>2</sub> at  $450^\circ\text{C}$  for 4 h. The maximum temperature and heating rate of  $450^\circ\text{C}$  and  $1^\circ\text{C min}^{-1}$  applied during activation are set to avoid sintering and agglomeration of the metal on the catalyst and therefore gain maximum catalyst performance. H<sub>2</sub> gas was feed through a saturator containing n-Heptanes (99.33 wt %, Sigma-Aldrich). The H<sub>2</sub> and n-C<sub>7</sub> flow rates ranged from  $20\text{--}45\text{ ml.min}^{-1}$  and  $0.287\text{--}0.686\text{ ml.min}^{-1}$  respectively and the experimentally determined molar composition of n-C<sub>7</sub> in the feed was 1.436 mol % and was calculated from extrapolated response factor values of n-C<sub>7</sub> by testing the feed total area on the GC-FID for blank runs across flow rates of  $20\text{--}72\text{ ml min}^{-1}$ . This compared well to the theoretical molar composition calculated from the standard vapor pressure of n-C<sub>7</sub> at  $0^\circ\text{C}$  and confirms the saturator is working very close to the theoretical optimum for a range of H<sub>2</sub> flow rates. The catalysts were tested at constant pressure (100 kPa), and temperatures ranging from  $250\text{--}400^\circ\text{C}$ .

The permeation of product mixtures gases across MCM-48 composite membranes were measured by the variable volume-constant pressure method in which the permeated gases at a feed pressure of 100 kPa at 298 K [25] was analyzed using Varian 3400 GC-FID fitted with a 50 m x 0.32 mm ID Al<sub>2</sub>O<sub>3</sub> capillary column.

## RESULTS AND DISCUSSION

**Characterization of the synthesized materials**

The small angle XRD patterns of MCM-48 membranesamples calcined at 500 °C for 4 hare shown in (Figure 3) which displayed an intense diffraction peak (1 0 0) at about 2θ of 2.53° for MCM-48 and 2.56° for 1% (Pt-Ni-Co)/MCM-48), which is characteristic of a mesostructure. Moreover, two additional peaks were observed in the XRD patterns, which can be indexed as (2 1 1) and (2 2 0). Two reflection peaks at 2θ smaller than 3° and a series of weak peaks in the range 3.5°–5.5°, are indexed to the Ia3d cubic structure. The peaks obtained in this study match very well with the similar peaks reported in the literatures [26-28]. The results in (Table 2), demonstrate the periodic ordered structure of MCM-48.

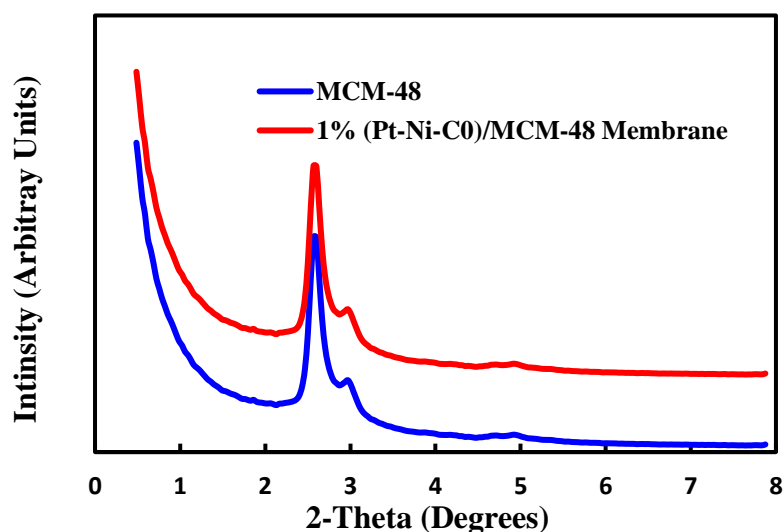


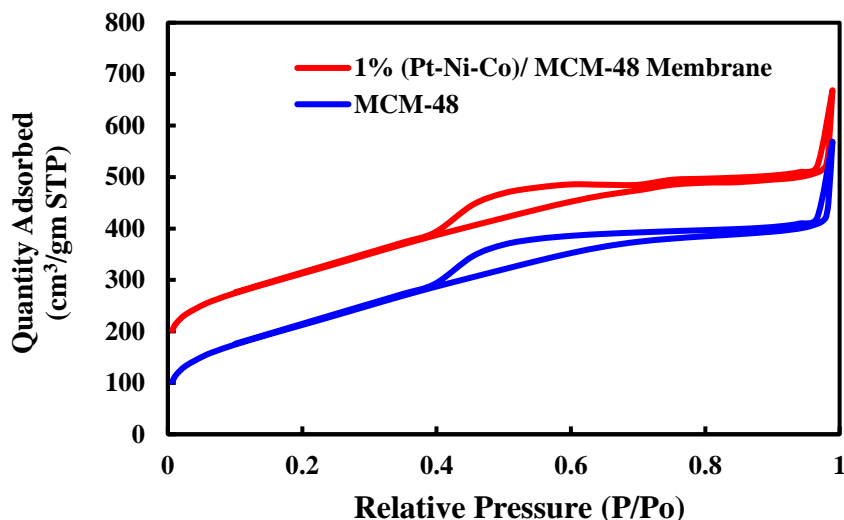
Figure (3) X-ray diffraction pattern of MCM-48 and 1% (Pt-Ni-Co)/MCM-48 Membrane.

Table (2) Physicochemical properties of MCM-48.

Sample	S <sub>BET</sub> (m <sup>2</sup> /g)	V <sub>P</sub> (cm <sup>3</sup> /g)	V <sub>μP</sub> (cm <sup>3</sup> /g)	D <sub>P</sub> (nm)	α <sub>o</sub> (nm)	t <sub>wall</sub> (nm)
MCM-48	1412	1.26	0.36	3.5	4	0.5
1%(Pt-Ni-Co)/MCM-48Catalytic membrane	850	0.812	0.05	3.1	3	0.3

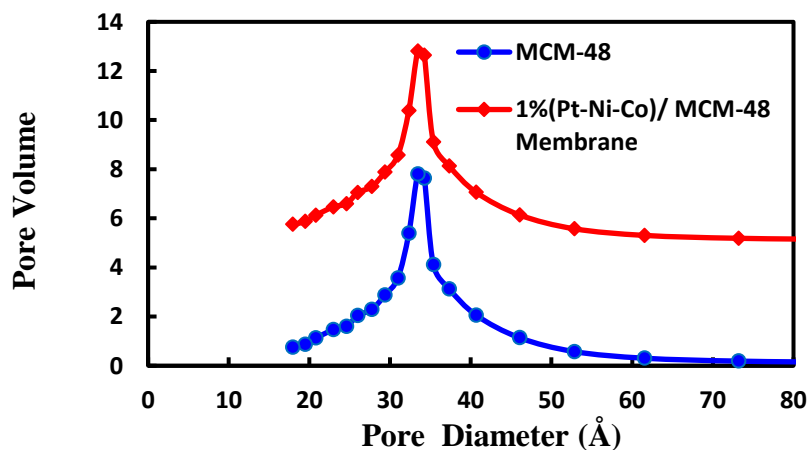
The nitrogen adsorption isotherms of MCM-48 corresponds to a type IV isotherm and a hysteresis loop type H1. Figure (4); hysteresis loops with sharp adsorption and desorption branches are indicative of a narrow pore size distribution. In general, for mesoporous molecular sieves, the sharpness and height of the capillary condensation step in the isotherms indicate the pore-size uniformity. From Figure (4) it can be found that the MCM-48 exhibits a typical type IV isotherm, with a typical capillary condensation step into uniform mesopores in the relative pressure (P/P<sub>0</sub>) range 0.05–0.25. The structural

parameters calculated from nitrogen adsorption measurements are presented in Table (2), which shows the specific surface area, pore volume, pore size and wall thickness of the sample.



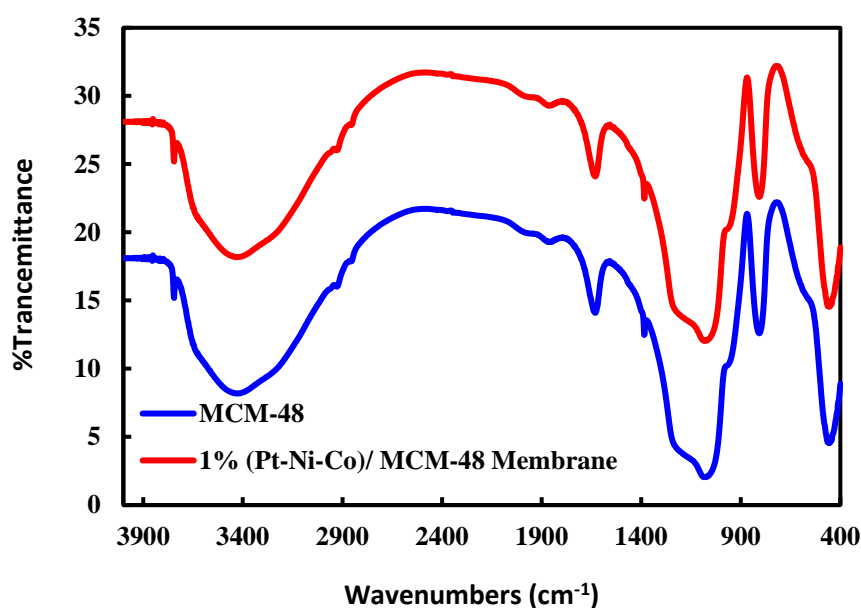
Figure( 4)Nitrogen adsorption desorption isotherms for MCM-48 and 1% (Pt-Ni-Co)/MCM-48 Catalytic membrane.

Figure (5) illustrates the pore size distribution (PSD) of MCM-48 and 1% (Pt-Ni-Co)/MCM-48 Catalytic membrane. The broad pore size distributions centered at 34 Å for the material synthesised using CTAB: NaOH: TEOS. A larger volume of mesopores was present for the basic preparation which gave the most pronounced pore size distribution and exhibited a very regular arrangement [14-15, 22- 23].



**Figure (5) BJH pore size distribution of MCM-48 and 0.1% (Pt-Ni-Co)/MCM-48 catalytic membrane.**

Figure 6 shows the FT-IR spectra of MCM-48, which contains the typical Si–O–Si bands around 1082, 964, 799 and 460  $\text{cm}^{-1}$ , which arise from the Si O Si stretching vibration. The absorption band at around 960  $\text{cm}^{-1}$  can be assigned to either Si OH or Si O Si stretching vibrations. The broad band at around 3463  $\text{cm}^{-1}$  is due to the presence of surface OH groups with strong hydrogen-bonding SiOH group's interactions between them. Finally the band at around 1637  $\text{cm}^{-1}$  can be assigned to the deformation modes of OH bonds of adsorbed  $\text{H}_2\text{O}$  [24-25]. A loaded metal (Pt-Ni-Co) exhibits a very similar spectrum to MCM-48 due to its low metals content, whereas two additional bands at 660 and 570  $\text{cm}^{-1}$  (black arrows) is appear in spectrum. The (Pt-Ni-Co)/MCM-48 bands for metals are slightly more intense than for MCM-48. We attribute this to the presence of larger Particles on the external surface of the pores for (Pt-Ni-Co)/MCM-48 also exhibits the same absorbance bands, with progressively increasing intensity [26].



**Figure (6) FT-IR spectra of MCM-48 and 1% (Pt-Ni-Co)/MCM-48 Membrane.**

#### SEM and EDAX of catalytic membrane reactor

SEM and EDAX characterisation techniques were performed on the prepared MCM-48 and 1% (Pt-Ni-Co)/MCM-48. SEM images for both of these materials can be seen in Figure (7) and Figure (8) at magnifications of 1000.

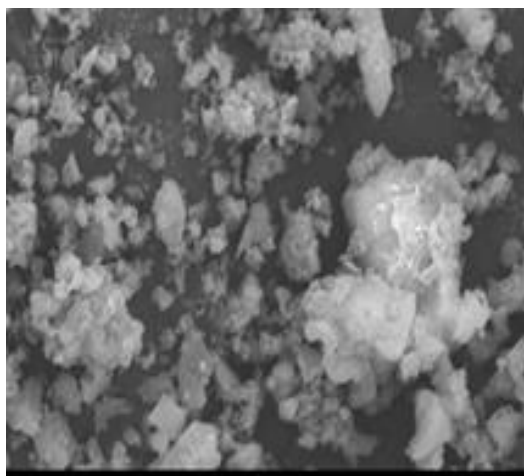


**Figure (7) SEM image of MCM-48 at a magnification of 1000.**

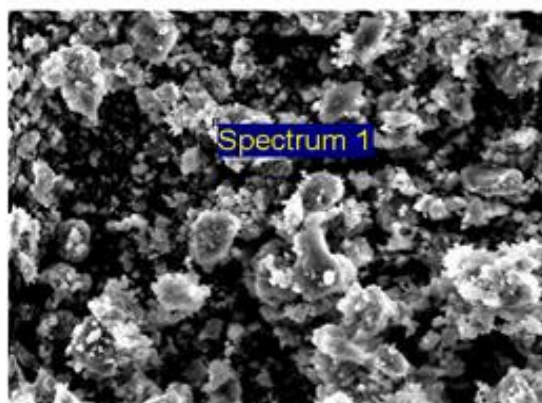
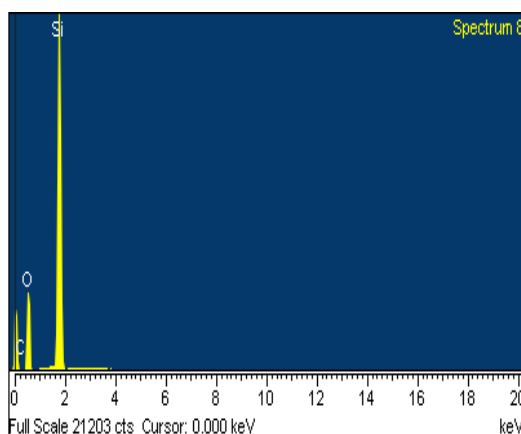


**Figure (8) SEM image of 1% (Pt-Ni-Co/MCM-48) at a magnification of 1000.**

EDAX was performed on the pre-tested catalyst sample. Typical EDAX images for MCM-48 and 1% (Pt-Ni-Co)/MCM-48 can be seen in Figure (9 and 10) respectively. The peaks from the EDAX graph resulting from the MCM-48 Nano porous material indicated that the zeolite was composed of C, O, Si and Al. while the resulting peaks from the Figure (10) representing the metals loaded. EDAX graphs were generated for several different points on the SEM images in order to gain correct average wt. % values for each of the components. From the Si and Al weight percentages deduced from these graphs, it is possible to gain an approximate value of the Si/Al ratio of the MCM-48 sample tested here. The Si/Al ratio was found to be approximately 6.24.



Figure(9) Typical EDAX image for MCM-48.

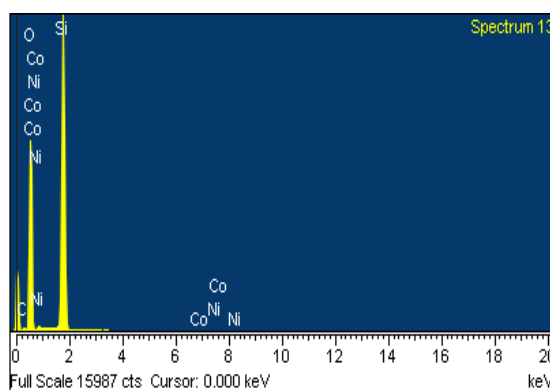


Figure (10) Typical EDAX image for 1% (Pt-Ni-Co)/MCM-48.

### Conversion of n-heptane

The total conversion in wt. % was calculated for the 1 % (Pt-Ni-Co) / MCM-48 catalytic membrane at different temperature maintaining a constant flow rate of 20 ml min<sup>-1</sup> from the following Equation.

$$\text{Conversion (n C 7 wt\%)} = \frac{[n C_7 \text{ in (g)}] - [n C_7 \text{ out (g)}]}{[n C_7 \text{ in (g)}]} \times 100\% \quad \dots (1)$$

Figure (11) shows the calculated conversion for the 1% (Pt-Ni-Co)/MCM-48 catalytic membrane tested at different temperatures for a constant n-C<sub>7</sub> flow rate of 0.287 ml/ min. The MCM-48 catalytic membrane does show activity which results from the presence of Lewis acid sites within the structure of the catalyst. 1% (Pt-Ni-Co)/MCM-48 catalytic membrane demonstrates the next highest conversion at higher temperatures with a conversion approach 83% at 400 °C. Tri-metallic 1% (Pt-Ni-Co)/MCM-48 may be found to have higher activity as a membrane reactor due to the metal cluster size.

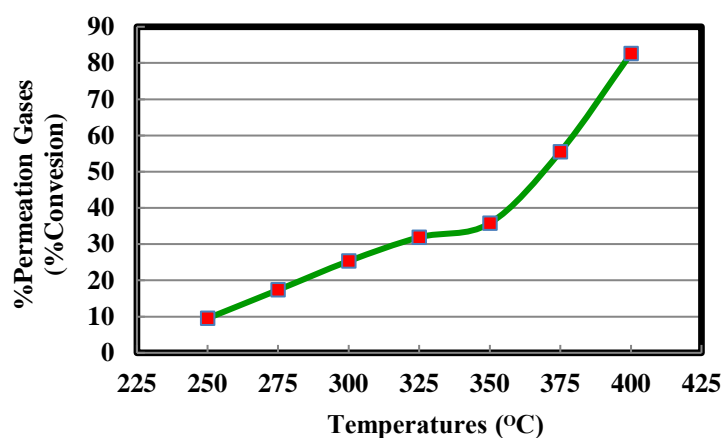


Figure (11) Conversion of n-heptane for the tested catalytic membrane.

**Selectivity to Isomerisation**

Figure (12) shows the selectivity to isomerisation products (i-C<sub>7</sub>) for 1% (Pt-Ni-Co)/MCM-48 catalytic membrane was calculated from the following equation.

$$\begin{aligned}
 & \text{Selectivity to Isomerisation ( wt\%)} \\
 & = \frac{\sum i - C_7(g)}{\sum \text{Total Products}(g)} \times 100\% \quad \dots (2)
 \end{aligned}$$

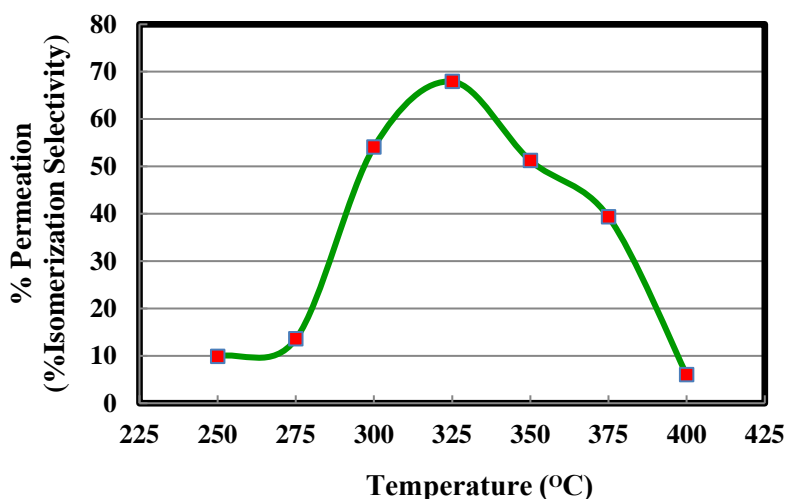


Figure (12) Isomerization product selectivity for the tested catalytic membrane.

Figure (12) displays the selectivity to isomerisation products for 1% (Pt-Ni-Co)/MCM-48 catalytic membrane in a membrane reactor at different operating temperatures. The Lewis acid sites of the zeolite allow for the transformation of intermediate alkenes into their structural isomers during the reaction mechanism

for isomerisation over Tri-functional catalysts. Without these acid sites, as on MCM-48, only dehydrogenation and hydrocracking reactions can occur [29]. The larger pores MCM-48 catalytic membrane result in poor selectivity to isomerisation products and are therefore not product selective. For example, cyclohexane with a molecular diameter of 0.6 nm is 6 times smaller than the pore diameter of MCM-48 with 3.5 nm, therefore the reactant molecules react and exit the catalytic pores before any selectivity can occur [30].

### Selectivity to Cracking

The selectivity to cracked products ( $C_1 - C_6$ ) was calculated for the 1% (Pt-Ni-Co) / MCM-48 catalytic membrane at all the tested temperatures for an n-C<sub>7</sub> flow rate of 0.287 ml.min<sup>-1</sup> by equation

$$\begin{aligned} \text{Selectivity to Cracking (wt\%)} \\ = \frac{\sum \text{Cracked Product (g)}}{\sum \text{Total Products (g)}} \times 100\% \quad \dots (3) \end{aligned}$$

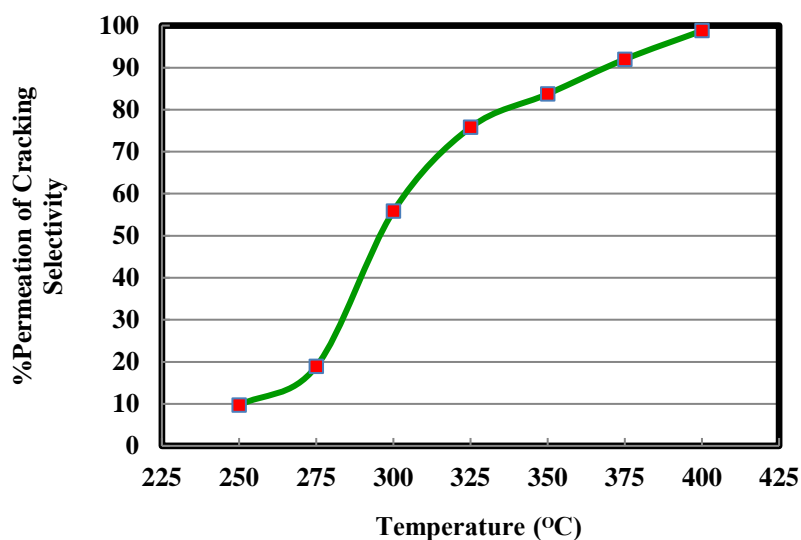


**Figure (13) Cracking product selectivity for the tested catalytic membrane.**

Figure (13) displays the results for selectivity to cracking 1% (Pt-Ni-Co)/MCM-48 catalytic membrane at tested temperatures. From this figure it is evident that the selectivity to cracking on shows an increase in selectivity up to 98wt % at 400°C. Here the MCM-48 catalytic membrane exhibits a greater selectivity for cracked products, again due to their pore structure and the presence of Lewis acid sites on the catalyst. Although the MCM-48 catalytic membrane is active, they are not structurally selective to desired isomerisation products for the hydroisomerisation of n-C<sub>7</sub> and have no Brønsted acid sites which aid isomerisation. Hydroisomerisation reactions occur in thermodynamic equilibrium with hydrocracking reactions as proved in literature [30] and typically occur at relatively low temperatures of 210-270°C. The MCM-48 catalytic membrane is

not active at the low temperatures required for hydroisomerisation and therefore displays no selectivity to isomerisation products. However the MCM-48 catalytic membrane shows high selectivity for cracked products due to the high operating temperatures of 300 – 400 °C and again due to the presence of Lewis acid sites within the structure of the catalyst.

### CONCLUSIONS

1. The use of MCM-48 catalytic membrane provides a promising alternative to conventional hydroisomerization and hydrocracking reactions.
2. The deposition of MCM-48 based thin protective layer on Al<sub>2</sub>O<sub>3</sub> membrane may increase the stability of the membrane under realistic conditions.
3. This membrane reactor system can be applied for other reactions such as dehydrogenation.
4. Due to its large pores relative to isomerisation products and lack of Brønsted acid sites MCM-48 was found to have no shape selectivity towards isomerisation products
5. 1 % (Pt-Ni-Co)/MCM-48 zeolitic catalytic membrane reactor showed good selectivity to cracked products due to the existence of Lewis acid sites on the catalysts.

### ACKNOWLEDGEMENTS:

Dr. Talib M. Albayati is grateful to both the University of Technology, Republic of Iraq, for allowing postdoctoral leave and to Manchester Metropolitan University, United Kingdom, for financial support.

### REFERENCES

- [1]. Frost&Sullivan, San Antonio, Oil Refining Technologies - New developments and growth opportunities, TX 78229, USA (26 May 2004).
- [2]. Van de Graaf, J.M., Zwiep, M., Kapteijn, F. and Moulijn, J.A., Application of a silicalite-1 membrane reactor in metathesis reactions, *Applied Catalysis A: General*. 178(2), (1999), 225-241
- [3]. Juergen Caro, Manfred Noack. Review Zeolite membranes – Recent developments and progress. *Microporous and Mesoporous Materials* 115 (2008) 215–233.
- [4]. Medina, S. Li, Z. Li, D. C. Lew, Y. Yan, Organic-functionalized pure silica-zeolite MFI low-k films. *Chem. Mater.* 17 (2005) 1851-1854.
- [5]. Medina, Z. Li, C.M. Lew, S. Li, D.I. Y. Yan, Pure-silica-zeolite MEL low-k films from nanoparticle suspensions. *J. Phys. Chem. B* 109 (2005) 8652-8658.
- [6]. Vilaseca, M. J. Coronas, A. Cirera, A. Cornet, J.R. Morante, J. Santamaria, Use of zeolite films to improve the selectivity of reactive gas sensors *Catalysis Today*, Volume 82, Issues 1–4, 30 July 2003, Pages 179-185.
- [7]. Coronas, J. J. Santamaria, The use of zeolite films in small-scale and micro-scale applications. *Chemical engineering science* 59 (2004) 4879-4885.
- [8]. Ruiz, A.Z. H. Li, G. Calzaferri, Organizing Supramolecular Functional Dye-Zeolite Crystals. *Angew. Chem. Int. Ed.* 45 (2006) 5282.
- [9]. Kim, H.S. S.M. Lee, K. Ha, C. Jung, Y.-J. Lee, Y.S. Chun, D. Kim, B.K. Rhee, K.B. Yoon, Aligned Inclusion of Hemicyanine Dyes into Silica Zeolite

- Films for Second Harmonic Generation. *J. Am. Chem. Soc.* 126 (2004) 673-682.
- [10]. Snyder, M.A. M. Tsapatsis, Hierarchical nano-manufacturing: from shaped zeolite nanoparticles to high performance separation membranes. *Angew. Chem. Int. Ed.* 46 (2007) 7560-7573.
- [11]. Davis M. E., Ordered porous materials for emerging applications. *Nature* 417 (2002) 813-821.
- [12]. Tsapatsis, M. Molecular sieves in the nanotechnology era *AIChE J.* 48 (2002) 654-660.
- [13]. Zhao, X. S.; Lu, G. Q. *Nanoporous Materials Science and Engineering*, Imperial College Press, London, 2004, Chapter 1.
- [14]. Kresge, C. T., Leonowicz, M. E., Roth, W. J., Vartuli, J. C., and Beck, J. S. Ordered mesoporous molecular sieves synthesized by a liquid-crystal template mechanism, *Nature* 359 (1992) 710-712.
- [15]. Olkhoviyk, O., Antochshuk, V., Jaroniec, M., Benzoylthiourea-modified MCM-48 mesoporous silica for mercury (II) adsorption from aqueous solutions. *Colloids and Surfaces A: Physicochemical and Engineering Aspects.* 236 (2004) 69-72.
- [16]. Pedernera, M. O. de la Iglesia, R. Mallada, Z. Lin, J. Rocha, Cronas, J. Santamaria, Preparation of stable MCM-48 tubular membranes. *Journal of Membrane Science* 326 (2009) 137-144.
- [17]. Ghiaci, M. R. Kia, A. Abbaspur, F. Seyedeyn-Azad, Adsorption of chromate by surfactant-modified zeolites and MCM-41 molecular sieve. *Separation and Purification Technology* Volume 40, Issue 3, 15 December 2004, Pages 285-295.
- [18]. Hudson, S.P. R.F. Padera, R. Langer, D.S. Kohane, The biocompatibility of mesoporous silicates. *Biomaterials* 29 (2008) 4045-4055.
- [19]. Mellaerts, R. R. Mols, J.A.G. Jammaer, C.A. Aerts, P. Annaert, J.V. Humbeek, G. Van den Mooter, P. Augustijns, J.A. Martens, Increasing the oral bioavailability of the poorly water soluble drug itraconazole with ordered mesoporous silica. *Eur. J. Pharm. Biopharm.* 69 (2008) 223-230.
- [20]. Rosenholm, J.M. A. Meinander, E. Peuhu, R. Niemi, J.E. Eriksson, C. Sahlgren, M. Lindén, Targeting of porous hybrid silica nanoparticles to cancer cells. *ACS Nano* 3 (2009) 197-206.
- [21]. Blumen S.R., Cheng K., Ramos-Nino M.E., Taatjes D.J., Weiss D, Landry CC, Mossman B.T. Unique mechanisms of uptake of acid-prepared mesoporous spheres (APMS) by lung epithelial and mesothelioma cells. *Am. J. Respir. Cell Mol. Biol.* 36, (2006) 333-342.
- [22]. Taralkar, U.S. M.W. Kasture, P.N. Joshi, Influence of synthesis condition on structure properties of MCM-48, *J. Phys. Chem. Sol.* 69 (8) (2008) 2075-2081.
- [23]. Doyle, A. M. B.K. Hodnett. Synthesis of 2-cyanoethyl-modified MCM-48 stable to surfactant removal by solvent extraction: Influence of organic modifier, base and surfactant, *Microporous and Mesoporous Materials* 58 (2003) 255-261.
- [24]. Doyle, A.M. E. Ahmed, B.K. Hodnett, The evolution of phases during the synthesis of the organically modified catalyst support MCM-48, *Catalysis Today* 116 (2006) 50-55.

- [25]. Hagg MB, Lie JA, Lindbrathen A. Carbon molecular sieve membranes: a promising alternative for selected industrial applications. *Ann N Y AcadSci* 2003; 984:329–45.
- [26]. Hyung-Ju Kim, Kwang-Suk Jang, Peter Galebach, Christopher Gilbert, Geoffrey Tompsett, W. Curtis Conner, Christopher W. Jones, Sankar Nair. Seeded growth, silylation and organic/water separation properties of MCM-48 membranes. *Journal of Membrane Science* 427 (2013) 293–302.
- [27]. Vetrivel, S. A. Pandurangan. Co and Mn impregnated MCM-41: their applications to vapour phase oxidation of isopropyl benzene. *Journal of Molecular Catalysis A: Chemical, Volume 227, Issues 1–2, (2005) 269-278.*
- [28]. Shao, Y.; Wang, L.; Zhang, J.; Anpo, M. Synthesis of hydrothermally stable and long-range ordered Ce-MCM-48 and Fe-MCM-48 materials. *J. Phys. Chem. B* 2005, 109, 20835.
- [29]. Eswaramoorthi, I., Lingappen, N. (2003). Ni-Pt/H-Y Zeolite Catalysts for Hydroisomerisation of n-C6 and n-C7, *Cat Let*, 87, 133-142.
- [30] Dwyer, J. Zeolite Structure, Composition and Catalysis. *Chemistry and Industry*, (1984) 258-269.